JCTC Journal of Chemical Theory and Computation

Article

pubs.acs.org/JCTC

The Mössbauer Parameters of the Proximal Cluster of Membrane-Bound Hydrogenase Revisited: A Density Functional Theory Study

Shadan Ghassemi Tabrizi,[†] Vladimir Pelmenschikov,[†] Louis Noodleman,[‡] and Martin Kaupp*[,†]

[†]Technical University of Berlin, Institute for Chemistry and Theoretical Chemistry, Sekr. C7, Strasse des 17. Juni 135, 10623 Berlin, Germany

[‡]Department of Integrative Structural and Computational Biology, The Scripps Research Institute, 10550 North Torrey Pines Road, CB213, La Jolla, California 92037, United States

Supporting Information

ABSTRACT: An unprecedented [4Fe-3S] cluster proximal to the regular [NiFe] active site has recently been found to be responsible for the ability of membrane-bound hydrogenases (MBHs) to oxidize dihydrogen in the presence of ambient levels of oxygen. Starting from proximal cluster models of a recent DFT study on the redox-dependent structural transformation of the [4Fe-3S] cluster, ^{57}Fe Mössbauer parameters (electric field gradients, isomer shifts, and nuclear hyperfine couplings) were calculated using DFT. Our results revise the previously reported correspondence of Mössbauer signals and iron centers in the $[4Fe\text{-}3S]^{3+}$ reduced-state proximal cluster. Similar conflicting assignments are also resolved for the $[4Fe\text{-}3S]^{5+}$ superoxidized state with particular regard to spin-coupling in the broken-symmetry DFT calculations. Calculated ^{57}Fe hyperfine coupling (HFC) tensors expose discrepancies in the experimental set of HFC tensors and substantiate the need for additional experimental work on the magnetic properties of the MBH proximal cluster in its reduced and superoxidized redox states.

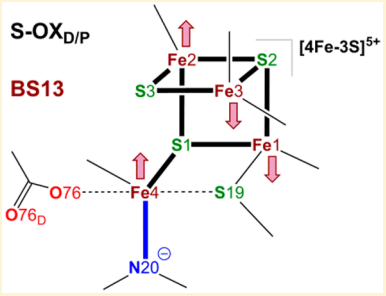

1. INTRODUCTION

Membrane-bound [NiFe]-hydrogenases (MBHs) from organisms like *Aquifex aeolicus* (*Aa*), *Escherichia coli* (*Ec*), *Hydrogenovibrio marinus* (*Hm*), or *Ralstonia eutropha* (*Re*) are capable of catalyzing the oxidation of H_2 at ambient levels of O_2, which acts as the terminal electron acceptor.[1−4] The oxygen tolerance of these enzymes has been traced to the replacement of a conventional [4Fe-4S] cubane in the O_2-inactivated [NiFe]-hydrogenases by an extraordinary [4Fe-3S] cluster at a distance of ∼11 Å to the active site.[5−7] Whereas all four iron centers in this [4Fe-3S] "proximal" cluster are still each coordinated by a cysteinate side chain (as in the cubane-type [4Fe-4S] present in O_2-sensitive [NiFe] hydrogenases), one inorganic μ_3-sulfide is replaced by two "supernumerary" cysteinates: Cys19 bridges Fe1 and Fe4 (numbering for *Re*-MBH[6] and *Ec*-MBH[7] unless otherwise stated) and Cys120 binds terminally to Fe3 (Figure 1). In the catalytic cycle, the proximal cluster switches between its reduced (RED[8]) and its oxidized state (OX). The RED/OX states, $[4Fe\text{-}3S]^{3+}/[4Fe\text{-}3S]^{4+}$, are formally equivalent to the $[4Fe\text{-}4S]^{+}/[4Fe\text{-}4S]^{2+}$ redox states of the conventional systems. However, the special constitution of the MBH proximal cluster confers considerable structural flexibility, which allows the attainment of a superoxidized $[4Fe\text{-}3S]^{5+}$ state (S-OX) at physiological redox potentials, a crucial feature for oxygen tolerance. In terms of the electron count, the superoxidized state corresponds formally to the $[4Fe\text{-}4S]^{3+}$ oxidized state of high-potential iron−sulfur proteins and experiences stabilization from the formation of a bond between the deprotonated backbone amide of Cys20 and Fe4 (Figure 1).[5] Upon binding of O_2 to the bimetallic [NiFe] active site, the quick delivery of *two* electrons from the proximal cluster[9] can thus prevent the formation of detrimental Ni-A oxygen species at the active site that would reactivate very slowly under physiological conditions.[10−13] The possible absence of stabilization by spin-dependent delocalization (double-exchange)[14] between iron centers of mixed-valent (MV) pairs (i.e., Fe^{2+}-Fe^{3+}) in all three redox states due to the asymmetry of the [4Fe-3S] cluster ("trapped valences") has been proposed as a complementary explanation for the strikingly small potential difference (<220 mV) between the reduced/oxidized and oxidized/superoxidized redox pairs in MBH.[15]

A recent computational study[16] rationalized the reversible redox-dependent RED ⇌ S-OX structural transformation of the proximal cluster at the three physiologically accessible $[4Fe\text{-}3S]^{3+/4+/5+}$ redox levels and reproduced the observed ^{14}N hyperfine couplings (HFCs)[17−19] of the Fe4-bound Cys20 amide (cf. Figure 1). Two previous combined experimental/DFT studies by Volbeda et al.[7] and Pandelia et al.[20] have tackled the problem of establishing a correlation between Fe sites from Mössbauer spectroscopy[9,20] and the S-OX proximal cluster molecular structure. The cited works disagree on the electronic structure of S-OX, and consequently, there is no consensus on the identity of ^{57}Fe Mössbauer centers with respect to Fe centers in the molecular structure.[21,22] The identity of Fe sites and spin coupling has also been addressed

Received: September 4, 2015
Published: November 23, 2015

DOI: 10.1021/acs.jctc.5b00854
J. Chem. Theory Comput. 2016, 12, 174−187

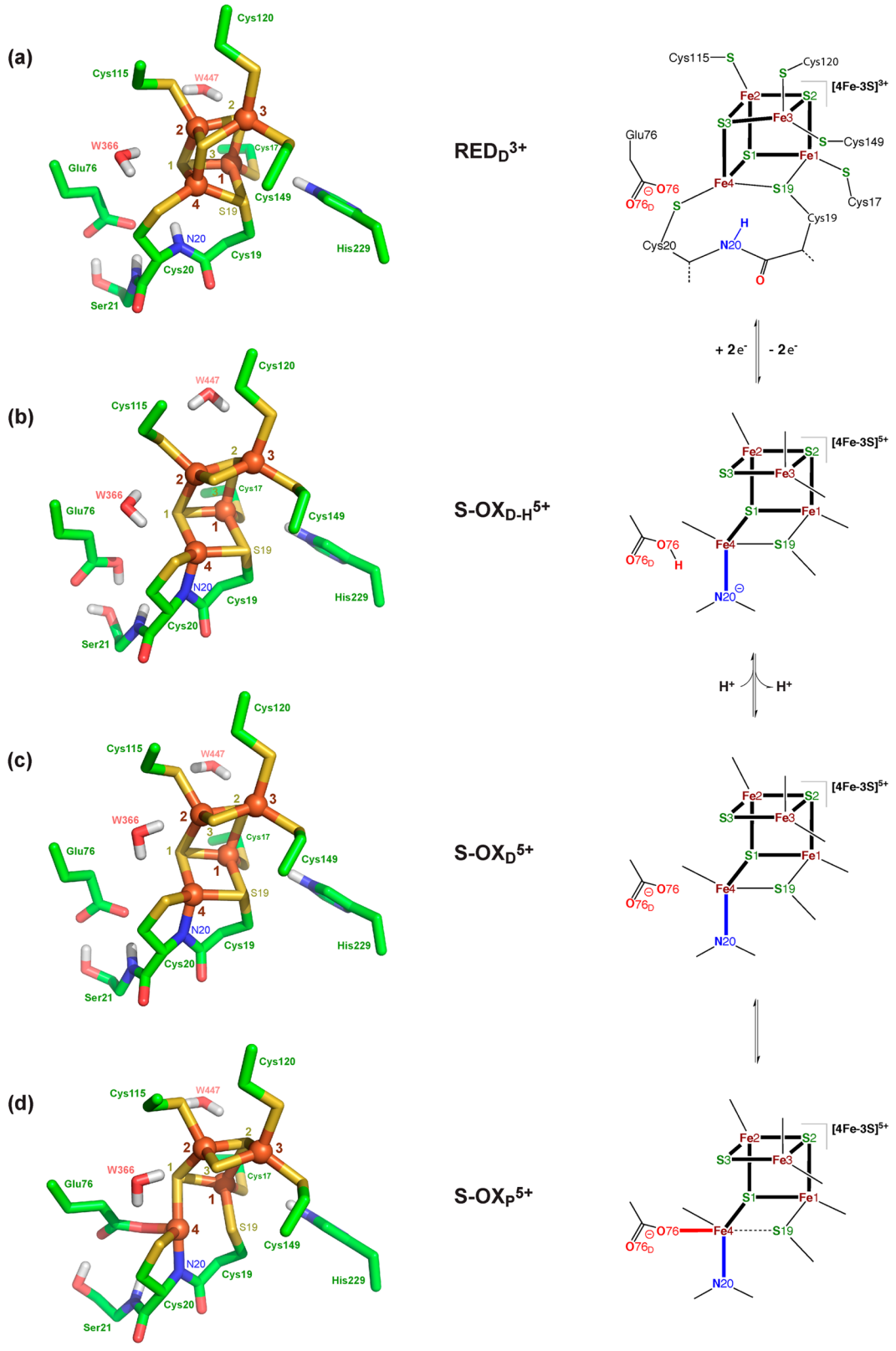

Figure 1. Optimized models (left) of the *Re*-MBH proximal cluster from ref 16 and their schematic representations (right). From top to bottom: the $[4Fe\text{-}3S]^{3+}$ reduced state RED_D^{3+} (a) and the $[4Fe\text{-}3S]^{5+}$ superoxidized states $S\text{-}OX_{D\text{-}H}^{5+}$ (b), $S\text{-}OX_D^{5+}$ (c), and $S\text{-}OX_P^{5+}$ (d). The inorganic iron–sulfur core atoms and residue numbering corresponds to the PDB 3RGW X-ray structure.[6] Only acidic hydrogen atoms are shown for clarity. In schematic representations, serine-21, histidine-229, and the water molecules W 366 and 447 were omitted for clarity. All of the models were optimized using PBE/lacv3p** for the broken-symmetry state BS13.

for the reduced-state $[4Fe\text{-}3S]^{3+}$ cluster.[20] However, severe doubts are in order regarding the DFT-optimized reduced-state structure proposed in ref 20 on account of calculated Mössbauer parameters: the computational model differs

DOI: 10.1021/acs.jctc.5b00854
J. Chem. Theory Comput. 2016, 12, 174–187

fundamentally from available X-ray crystal structures as the bond between Fe3 (in the present *Re*- and *Ec*-MBH numbering), one of the supernumerary cysteinates, Cys120, is ruptured, and the Fe3−Fe4 distance is contracted from 3.98 to 2.81 Å.

Here, we take an objective and comprehensive point of view of prior computational and experimental work in reporting a detailed reinvestigation of electronic structure and Mössbauer parameters of the proximal cluster in reduced and superoxidized states.

The disagreement on the S-OX electronic structure is clearly resolved, making the interpretation in terms of a match between Mössbauer spectroscopic and structural Fe centers unambiguous. For the reduced state, we demonstrate that a reasonable match with experimental Mössbauer parameters is possible for a model that agrees excellently with X-ray data. On the basis of our calculations, we suggest that a reevaluation of magnetic Mössbauer spectra with respect to hyperfine structure, or the highly desirable performance of ENDOR experiments, may lead to major revisions of the experimentally reported ^{57}Fe hyperfine tensors for both (paramagnetic) redox states of the proximal cluster.

2. BRIEF SUMMARY OF PREVIOUS EXPERIMENTAL/COMPUTATIONAL STUDIES OF MÖSSBAUER PARAMETERS AND ELECTRONIC STRUCTURE

The elementary features of the electronic structure of multinuclear open-shell transition metal clusters are the distribution of formal metal oxidation (and spin) states and the exchange (and double-exchange[23,24]) interactions between the metal ion spin centers. For elucidating the electronic structure of biological Fe−S clusters, ^{57}Fe Mössbauer spectroscopy is extremely helpful.[25−27] As density functional theory (DFT) has been shown to be capable of accurately predicting Mössbauer parameters, most importantly isomer shifts and nuclear quadrupole splittings,[28−31] theoretical calculations can help to link "spectroscopic metal centers" to site-specific iron centers in the molecular structure. Using broken-symmetry density functional theory (BS-DFT), the choice of the BS state becomes crucial in the comparison between experiment and computation (see, for example, refs 7, 20, and 32).

Experimental/theoretical Mössbauer parameters of the proximal cluster of MBH published to date are summarized concisely in Table 1.

In a first zero-field Mössbauer spectroscopic investigation of *Aa*-MBH, Pandelia et al.[9] reported isomer shifts (δ), quadrupole splittings (ΔE_Q), and asymmetry parameters (η) for the four iron ions of the proximal cluster in its paramagnetic superoxidized redox state (S-OX, S = 1/2, formal metal oxidation states of [1Fe^{2+}, 3Fe^{3+}]), treating two ferric sites (δ = 0.26 mms^{-1}) as equivalent.[9] Volbeda et al.[7] employed these results in a combined crystallographic/computational study as a reference.

In a follow-up combined spectroscopic/theoretical study, Pandelia et al.[20] reported applied-field ^{57}Fe Mössbauer spectra, giving δ, ΔE_Q, and HFCs for all iron sites in the different paramagnetic clusters in H_2-reduced (RED proximal cluster, S = 1/2, [3Fe^{2+},1Fe^{3+}]) and superoxidized *Aa*-MBH. Experiments were complemented with DFT calculations. Apparently good agreement of calculated sets $\{\delta_i\}$, $\{\Delta E_{Q,i}\}$, and $\{\eta_i\}$ (i = 1−4 for Fe1−Fe4) for the reduced-state cluster with experiment was reached by Pandelia et al.[20] However, the optimized structure (see Table S8 in ref 20) does not resemble published X-ray structures[5−7] with the proximal cluster in its reduced redox state.

For the superoxidized state, Pandelia et al.[20] and Volbeda et al.[7] deduced different assignments of Mössbauer centers to Fe sites in their X-ray diffraction-based models. The local spin state

Table 1. Summary of Published Experimental[9,20] and Calculated[7,20] ^{57}Fe Mössbauer Parameters for the Reduced and Super-Oxidized *Aa*-MBH Proximal Cluster[a]

	site[b]	ΔE_Q (mms^{-1})[c]	δ (mms^{-1})	η	A_{iso} (MHz)
S-OX exp.[9]	S	2.41	0.46	N.A.	N.A.
		0.60	0.26	N.A.	N.A.
		0.60	0.26	N.A.	N.A.
		1.23	0.40	N.A.	N.A.
BS13 PC3^H calc.[7]	Fe1	+2.36	N.A.	0.21	+[d]
	Fe2	+0.31	N.A.	0.44	−[d]
	Fe3	−0.31	N.A.	0.29	+[d]
	Fe4	+0.96	N.A.	0.60	−[d]
S-OX exp.[20]	S	(+)2.45	0.46	0.5	+25.7
		(+)0.70	0.39	1.0	−47.9
		(+)0.60	0.28	0.3	+33.4
		(−)1.00	0.40	0.7	−33.6
Ox2_24 calc.[20]	Fe4	+2.25	0.38	0.40	+48.91
	Fe2	+0.81	0.30	0.74	−57.75
	Fe3	+0.74	0.22	0.56	+58.72
	Fe1	−1.56	0.39	0.83	−60.10
RED exp.[20]	S	+2.60	0.50	0.1	+19.30
		+0.84	0.42	0.3	−34.50
	F	+1.52	0.71	0.3	± 43.24[e]
		+1.23	0.44	0.9	∓27.63[e]
Red2_24 calc.[20]	Fe3	+2.13	0.46	0.51	+26.53
	Fe2	+0.93	0.36	0.30	−50.01
	Fe1	+1.41	0.60	0.28	−63.28
	Fe4	+1.25	0.35	0.99	+43.66

[a]Pairs of experimental and calculated data are arranged to have corresponding Fe sites matching row-wise, as assigned in the respective DFT studies. Calculations of $\{\Delta E_Q\}$ in ref 7 favored the so-called BS13 PC3^H model for S-OX (spin alignment corresponding to our BS13, explained in detail in section 3.2), referring to earlier Mössbauer data from ref 9. Pandelia et al. compared calculated Mössbauer parameters with experimental data reported in the same work,[20] favoring models Ox2_24 (corresponding to our BS34) for S-OX and Red2_24 (corresponding to our BS34) for RED. [b]Experimental site designations (S = "special", F = "ferrous") follow ref 20. The numbering of Fe sites in the DFT results follows the numbering for *Ec*-MBH[7] and *Re*-MBH,[6] which are the same. A different numbering for *Hm*-MBH was used in ref 20 but has been converted in the present table and also in the following work to the numbering of *Ec*- and *Re*-MBH as follows: Fe1 → Fe1, Fe2 → Fe4, Fe3 → Fe2, and Fe4 → Fe3. However, naming of the favored models in ref 20, Ox2_24 and Red2_24, has been retained. [c]Signs for nuclear quadrupole splittings $\{\Delta E_Q\}$ have not been determined in ref 9. In ref 20, the signs of the $\{\Delta E_Q\}$ could not be determined with full confidence for S-OX; reported signs (given in parentheses) followed the accompanying DFT calculations. [d]We assigned signs to the $\{A_{iso}\}$ based on a "classical" spin coupling scheme proposed by Volbeda et al.,[7] see Results section. [e]The caption to Table S6 of ref 20 indicates that Mössbauer spectra in applied magnetic fields could not resolve the signs of A_{iso} for two sites in the reduced-state cluster. Both alternative sets of the signs of $\{A_{iso}\}$ are given in the table; the lower sign option conforms to the DFT results in ref 20, and this sign option was thus chosen for the simulations.[20]

DOI: 10.1021/acs.jctc.5b00854
J. Chem. Theory Comput. 2016, 12, 174−187

of ferric Fe4 in model Ox2_24 (spin coupling corresponding to our BS34, see section 3.2) favored by Pandelia et al. was controversial, and a discussion on the best-suited broken-symmetry state for S-OX and the probable protonation state and conformation of the glutamate residue binding to (proximal) or in the vicinity of (distal) Fe4 ensued.[21,22]

We note in passing that a very recent structure determination by X-ray diffraction, vibrational and EPR spectroscopies, and quantum-chemical calculations for the superoxidized state of *Re*-MBH indicated a somewhat different structure where a hydroxyl ligand is coordinated to Fe1 and additionally accepts a hydrogen bond from His229.[18] Consideration of this proposed new species is outside the scope of the present computational Mössbauer study and will be addressed in a separate work.

3. COMPUTATIONAL DETAILS

3.1. Model Structures and Density-Functional Methods. Computational models for the reduced-state cluster were originally constructed[16] from the X-ray data for *Re*-MBH[6] (PDB ID: 3RGW). Coordinates of structures employed here for the calculation of Mössbauer and hyperfine parameters have been given partially in the Supporting Information of ref 16. However, for the present study, some additional DFT structure optimizations have been performed.

Full details of the employed optimization protocol were reported previously.[16] Briefly, structure optimizations without dispersion corrections, using the lacv3p** basis-set/Fe-pseudopotential combination,[33] and a polarizable continuum solvent model (dielectric constant ε = 4.0), were performed with the GAUSSIAN 09 program package.[34] Polypeptide α-carbon atoms were fixed in the optimizations except for the α-carbon of Cys20. Its deprotonated backbone amide binds to Fe4 in the superoxidized state, and it was thus left free to change (cf. ref 16). Structure optimizations including Grimme's D3 dispersion corrections[35,36] were carried out with Jaguar 7.8.[37] However, as the small structural changes affected computed Mössbauer parameters only slightly, we will largely report data obtained without dispersion corrections.

When the PBE functional[38,39] was used, deviations compared to X-ray structures in important bonding and nonbonding internuclear distances for the reduced-state proximal cluster (computational model RED_D^{3+}) amounted to ~0.1 Å at most (see also Figure 4 and Table S2 in ref 16). Importantly, the B3LYP[40,41] functional overestimated metal−ligand bond lengths compared to the X-ray reference. Here, we therefore discuss only the PBE structures. Calculations of Mössbauer parameters have nevertheless been carried out for some B3LYP structures as well (results are given in the Supporting Information).

For the present study of Mössbauer parameters, accurate single-point calculations at the optimized structures were performed using Turbomole 6.3.[42] We used an all-electron (15s11p6d)/[9s7p4d][43−45] basis set on Fe sites, shown previously to well-reproduce HFCs in transition metal complexes.[44,45] For all other atoms, the flexible IGLO-II[46] basis set was used. This basis-set combination will in the following be denoted as "EPRB". Solvent effects have been taken into account with the COSMO[47] conductor-like screening model (ε = 4.0). For these calculations, the PBE and the B3LYP functionals were used. Converged orbitals from Turbomole were exported to our in-house program MAG[48] to calculate EFGs (ΔE_Q, η), electron densities at the locations of the Fe nuclei (for the calculation of δ), and HFCs. Because of the strong dependence of calculated ^{57}Fe nuclear quadrupole splittings on the density functional used, which is especially pronounced for the reduced-state proximal cluster, certain structures/BS states (see next section) have also been optimized, and single-point calculations were carried out with customized hybrid functionals using 5% Hartree−Fock (HF) exchange (recommended by Szilagy and Winslow[49] for Fe−S clusters and used by Volbeda et al. in their work on the proximal cluster[7]) or 10% HF-exchange. The OLYP density functional,[40,50] which performed well in recent computations of Mössbauer parameters,[31,51] has been tested too. Optimizations and single-point calculations using OLYP were performed with GAUSSIAN 09, as the OLYP functional has not been implemented in Turbomole. SCF orbitals were subsequently transferred to MAG for the calculation of spectroscopic properties.

3.2. Broken-Symmetry States. Briefly, in the broken-symmetry approach, states are represented by single Kohn−Sham determinants with maximal local spin projections of the high-spin Fe^{2+} and Fe^{3+} centers, i.e., $|M_{S_i}| = S_i$. When '↑' ("net α") and '↓' ("net β") denote $M_{S_i} > 0$ and $M_{S_i} < 0$, there are essentially six configurations [2Fe↑:2Fe↓] given that the identity of Fe^{3+}/Fe^{2+} oxidation states is normally either lost during SCF convergence or there is a preference for localizing "the odd electron" on either of the centers of the MV pair. The proximal cluster of MBH is particularly asymmetrical in its superoxidized state. Following ref 16, we denote broken-symmetry states "BS*ab*". Here, *a* and *b* are the numbers of iron centers that have net β spin when $\sum_i M_{S_i} = 1/2$. A schematic representation of state BS13 of the superoxidized cluster is shown in Figure 2.

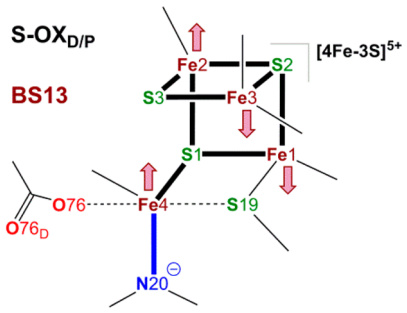

Figure 2. Schematic representation of the S-OX state BS13 with '↑' and '↓' arrows representing an excess of α and β spin densities, respectively, on the individual sites. The bond between the deprotonated backbone amide of Cys20 and Fe4 is drawn blue and bold. The dashed bonding implies alternative Fe4-S19/Fe4-O76 coordination in structures S-OX$_{D/P}$, respectively.

Our convention (indexing net β sites) for naming BS states concurs with that of Pandelia et al.,[20] but our numbering for the Fe atoms differs. For the reduced state, our BS designations differ from those of Mouesca et al.,[15] who chose to name BS states of the reduced state by the centers that have α-spin (with $\sum_i M_{S_i} = 1/2$). Our numbering of the Fe centers follows that for *Re*-MBH and *Ec*-MBH (see Figure 1), as used also in the DFT modeling in ref 16 (starting from X-ray structures of *Re*-MBH) and refs 7 and 15 (starting from X-ray structures of *Ec*-MBH; X-ray structures for *Aa*-MBH are not available as yet). The numbering of proximal-cluster iron centers for *Hm*-MBH

DOI: 10.1021/acs.jctc.5b00854
J. Chem. Theory Comput. 2016, 12, 174−187

employed in ref 20 can be converted to that for *Re*-MBH and *Ec*-MBH as follows: Fe1 → Fe1, Fe2 → Fe4, Fe3 → Fe2, and Fe4 → Fe3.

3.3. Calculation of Mössbauer Parameters. Details on ΔE_Q and η, and on calibration fits for the calculation of isomer shifts (using the recent test set by Sandala et al.[31]) are given in section 1 of the Supporting Information. We note that the results of a recent study[52] using relativistic calculations with finite-nucleus models likely give a more reliable slope than nonrelativistic point nucleus calculations, but some dependence on the DFT exchange-correlation potential can still be expected. Further, a fit to isomer shift data over multiple systems always provides a check on accuracy, see also ref 53. Computed η values will be disregarded here, as they are influenced too much by small structural inaccuracies to be diagnostic, and their extraction from the spectra is afflicted with more uncertainty than that of $\{\Delta E_Q\}$ and $\{\delta\}$. The ΔE_Q values are most diagnostic for bonding and spin-coupling, whereas the isomer shifts mainly reflect the pattern of formal oxidation states and covalency of the Fe sites. The sign of ΔE_Q can change by small perturbations when η is large, i.e., close to 1. ^{57}Fe HFCs in iron−sulfur complexes have been studied computationally for a long time.[54] However, quantitative DFT accuracy of the isotropic HFCs (A_{iso}) of transition metal sites is limited by core−shell spin polarization.[44] We have thus applied semiempirical scaling factors to the A_{iso} values calculated by DFT. The scaling factors were determined from a comparison with experimental isotropic HFCs for a set of 12 distinct Fe sites. Anisotropic HFC contributions depend less on core−shell spin polarization[55] and are thus reproduced without any scaling.

Alternatively, a semiempirical scheme developed by Mouesca et al.[54] is used, relying on an established approximate proportionality between Fe 3d Mulliken spin populations and ^{57}Fe HFCs.

More details on the calculation of A_{iso} for ^{57}Fe centers, including the calibration against experimental data, are given in section 5 of the Supporting Information.

3.4. Spin Projection. To compare computed HFCs to experimentally determined effective values, a two-step spin-projection scheme[56] has been employed. The $\mathbf{a}_i^{BS}(X)$ raw results are first converted to site tensors (that parametrize the hyperfine interaction of site spin $\mathbf{S}_i$ with nucleus X) as

$$\mathbf{a}_i(X) = \frac{S_t}{\pm S_i}\mathbf{a}_i^{BS}(X) \tag{0.0}$$

where S_t is the total spin quantum number (S_t = 1/2 for RED and S-OX). The sign in the denominator is determined by the projection of the site spin with respect to the projection of the total spin in the Kohn−Sham determinant representing the BS state. Conversion to effective HFCs in the coupled representation is given by the Wigner−Eckart projection theorem

$$\mathbf{A}_i(X) = \frac{\langle \mathbf{S}_i \cdot \mathbf{S}_t \rangle}{\langle \mathbf{S}_t \cdot \mathbf{S}_t \rangle}\mathbf{a}_i(X) \tag{0.1}$$

The ratio $\langle \mathbf{S}_i \cdot \mathbf{S}_t \rangle / \langle \mathbf{S}_t \cdot \mathbf{S}_t \rangle = \langle \mathbf{S}_i \cdot \mathbf{S}_t \rangle / S_t(S_t + 1) = K_i^t$ is called the spin-projection coefficient, thus

$$\mathbf{A}_i(X) = K_i^t \mathbf{a}_i(X) \tag{0.2}$$

The expectation values in eq 0.1 are understood to be taken in any one of the degenerate spin wave functions of the S_t = 1/2 doublet of interest. These scalar projection coefficients neglect local zero-field splitting (ZFS) interactions and assume that exchange coupling dominates over local ZFS interactions, as is often the case for Fe−S clusters.[24] The effective HFC tensors are of course "properties" of a certain doublet only.

A positive spin-projection coefficient indicates that the expectation value of the site-spin projection onto the direction of a weak magnetic field, applied along one of the principal axes of the system's g-tensor, has the same sign as the expectation value of the projection of the conserved total spin on the field direction. In certain cases, meaningful spin-projection coefficients can be derived by a simple analytical procedure once a formal coupling scheme has been devised (see below).[24,57,58] Because of ambiguities in choosing a coupling scheme, for S-OX, we have instead obtained spin-projection factors from a numerical diagonalization of the Heisenberg−Dirac-van-Vleck (HDvV) Hamiltonian, including also a delocalization term (see section 4 in the Supporting Information; eq 0.1 remains approximately valid due to the incipient valence localization). The resulting projection coefficients are very different from sets assumed previously.[7,16,20]

4. RESULTS AND DISCUSSION

4.1. Molecular Structures. *a. S-OX State.* Three possible structures of the S-OX proximal cluster (S-OX$_{D\text{-}H}^{5+}$, S-OX$_D^{5+}$, and S-OX$_P^{5+}$) differ in the conformation (distal/proximal) and the protonation state of a glutamate residue (Glu76) close to the special iron Fe4. These DFT-optimized structures (in particular S-OX$_P^{5+}$ and S-OX$_D^{5+}$, see Figure 1) agree well[16] with the reference X-ray structures.[5,7] S-OX$_{D\text{-}H}^{5+}$ has protonated Glu76 in a distal position with respect to Fe4 and may represent the primary product of the redox-dependent structural transformation. Recently some of us have postulated a RED$_D^{5+}$ → S-OX$_{D\text{-}H}^{5+}$ structural transformation to follow two-electron oxidation of the RED$_D^{3+}$ reduced cluster.[16] Following proton transfer off the cluster complex, S-OX$_{D\text{-}H}^{5+}$ → S-OX$_D^{5+}$, the deprotonated glutamate residue can shift to bind to the special iron center, Fe4, S-OX$_D^{5+}$ → SOX$_P^{5+}$. This binding is slightly exothermic. Here, we have evaluated S-OX$_{D\text{-}H}^{5+}$, S-OX$_D^{5+}$, and S-OX$_P^{5+}$ as candidates to represent the HYSCORE-,[19] ENDOR-,[18] and Mössbauer spectroscopically[9,20] detected S-OX species. State BS12 yields the lowest energies for S-OX$_{D\text{-}H}^{5+}$, S-OX$_D^{5+}$, and S-OX$_P^{5+}$ in structure optimization using DFT.[16] The energetic differences between BS12 and BS13 structures however are small for all three S-OX candidates. Searching the S-OX potential energy surface for a minimum with Glu76 protonated at the carboxylate oxygen atom distal to the cluster and attached to Fe4 via the carbonyl oxygen atom had not been successful.[16] Our attempt using D3 dispersion corrections in the DFT optimizations also gave no structure analogous to model PC3^H by Volbeda et al.[7] (which we would call S-OX$_{P-H}^{5+}$). Despite differences in modeling (we use a pure QM approach whereas Volbeda et al. employed QM/MM methodology for optimization and extracted smaller QM models for the calculation of Mössbauer parameters), this raises concerns with respect to the stability of a structure like PC3^H.

b. RED State. The reduced-state model RED$_D^{3+}$ is in good agreement with available crystal structures for all BS states and represents the only structural model for the reduced state evaluated here. Although an alternative conformation (RED$_P^{3+}$)

DOI: 10.1021/acs.jctc.5b00854
J. Chem. Theory Comput. 2016, 12, 174−187

had been found to exist on the RED potential energy surface, the RED_P conformation is energetically competitive with RED_D only in the OX or S-OX redox states,[16] and it may thus be excluded for the present investigation.

4.2. Broken-Symmetry States and Iron Spin States. Relative energies of all six BS states considered for RED_D^{3+}, $S\text{-}OX_{D\text{-}H}^{5+}$, $S\text{-}OX_D^{5+}$, and $S\text{-}OX_P^{5+}$ are provided in Table S2. The PBE/EPRB single-point results differ only a little from those obtained directly at the PBE/lacv3p** optimization level, whereas the B3LYP/EPRB energy differences cover a somewhat larger range (particularly for BS24 and BS34, see below). All BS states for RED_D^{3+} lie within a rather small energy window of <4 kcal/mol for PBE and <6 kcal/mol for B3LYP. In contrast, the reduced-state models by Pandelia et al. display significantly larger ranges for the relative energies of up to ∼18 kcal/mol.[20] The largest "outliers" of this kind can be understood from a comparison of computed Mössbauer parameters (see below). For example, the high relative energy of 18.41 kcal/mol for their Red1_13 (PBE structure, B3LYP single point, spin-alignment corresponding to our BS12) may be explained by an unfavorable valence localization in the MV pair. The theoretical Mössbauer parameters calculated by Pandelia et al. show localization according to $Fe3^{2+}$-$Fe4^{3+}$ in the BS12 MV pair, whereas we obtain a much lower relative energy for BS12 with localization according to $Fe3^{3+}$-$Fe4^{2+}$. In our experience, the state with unfavorable localization would probably not remain stable during structure optimization.

Conversely, for the S-OX state at the level of structure optimization, BS14 and BS23 have energies ∼10 kcal/mol above the lowest state (BS12). We have therefore calculated Mössbauer parameters only for BS12, BS13, BS24, and BS34, which are close in energy. The six different BS configurations for both redox states of the cluster allow in principle different distributions of formal metal oxidation states, as *a priori* preferences of certain centers (or pairs) for certain oxidation states are not known. In contrast to the situation encountered for the reduced state (see section 4.3), for the superoxidized state the distributions of metal oxidation states within the pairs with the same relative alignments of site spins, BS12/BS34, BS13/BS24, and BS14/BS23, were interestingly found to be identical, as we explain now.

In iron−sulfur clusters, calculated Mulliken spin populations for Fe are often not very diagnostic. This deficiency is due to pronounced delocalization of spin density onto the sulfur atoms (as demonstrated in Table S2). Despite this potential pitfall, the conspicuously low spin population for Fe4 (almost one unit lower compared to the other sites) in states BS24 and BS34 of S-OX had been used to assign Fe4 as a ferrous high-spin site.[7,16]

Localization within the potential MV pairs Fe2-Fe4 and Fe3-Fe4 in states BS24 and BS34, respectively (selected as MV pairs in the initial guess), could indeed be expected from the cluster topology. That is, the Fe2−Fe4 and Fe3−Fe4 distances are the largest Fe−Fe distances in S-OX (∼4.0 Å and ∼5.6 Å, respectively), precluding direct overlap of Fe 3d orbitals. However, chemical intuition predicts a strong preference (lower energy) for the hard anionic nitrogen ligand (a good σ-donor) from the deprotonated backbone amide of Cys20 to bind to a ferric Fe4.[5,7] Interpreting spin populations in BS24 in terms of a ferrous Fe4 contradicts this expectation: all three BS24 S-OX candidates are (at PBE/lacv3p** level) at most 3.1 kcal/mol (for $S\text{-}OX_P^{5+}$) above the lowest BS12 state with an undisputedly ferric Fe4. Mouesca et al. have claimed[21] that the Ox2_24 state (spin-alignment corresponding to our BS34, i.e., Fe1 and Fe2 are '↑' and Fe3 and Fe4 are '↓' in the present numbering of Fe sites) favored by Pandelia et al. for S-OX has a ferrous Fe1 and a ferric Fe4, the latter with a local spin quantum number of $S_4 = 3/2$. Indeed, a diverse set of computational data supports this notion. Our analysis of Boys localized orbitals suggests a ferric Fe4 with a local *z*-projection of $M_{S_4} = -3/2$ in BS34 together with an Fe1-Fe2 MV pair. That is, compared to the initial guess, one electron has been transferred from the Fe3-Fe4 MV pair to the Fe1-Fe2 pair. At the PBE level, this is confirmed by the canonical molecular orbitals with the α HOMO being mainly a 3d orbital on Fe4 and the β HOMO having substantial contributions from Fe1 and Fe2 (with σ-bonding character between these sites). Matters are similar for BS24, where Fe4 also becomes ferric with a local projection $M_{S_4} = -3/2$. In contrast to state BS34, there is no valence delocalization in BS24 (Fe1 is ferrous and Fe3 is ferric, as confirmed by the MOs) due to the larger separation of the MV centers Fe1-Fe3. BS13 has a similarly localized MV pair as that of BS24. BS states BS12/BS34 and BS13/BS24 (and also BS14/BS23) are pairwise connected by having similar MV pairs. The two BS states of a pair may be regarded as different orbital configurations of each other that are interconverted by a spin-forbidden transition involving a spin-flip of one majority-spin electron at Fe4, starting from BS12 or BS13. This leads to $\sum_i M_{S_i} = -1/2$ for BS34 and BS24, respectively, with Fe4 being ferric with intermediate spin. This observation is reminiscent of the orbital configurations OS1, OS2, and OS3 for the oxidized $[4Fe\text{-}4S]^{3+}$ cluster of high-potential iron−sulfur proteins (HiPIP's).[24,59] Notably, a quantum mixture of $S_i = 3/2$ and $S_j = 5/2$ local spins for the two sites *i* and *j* of the ferric pair has been described for OS1 and OS2.[24] In the present cases, the cluster structure (large separation of the centers of the ferric pair) enforces localization, such that well-defined local spins of $S_3 = 5/2$ for BS34 and $S_2 = 5/2$ for BS24 may be combined for both BS34 and BS24, either with a quantum mixture of $S_4 = 3/2$ and $S_4 = 5/2$ or with a "pure" $S_4 = 3/2$.

Spin canting, i.e., a local $S_4 = 5/2$ with $|M_{S_4}| = 3/2$ (with the other site spins having maximal projections), cannot be described in the present collinear spin framework, ruling out a pure $S_4 = 5/2$. An interpretation in terms of $S_4 = 3/2$ in BS24 and BS34 is indicated by $\langle S^2 \rangle$ expectation values. For the BS Kohn−Sham determinants representing BS12 and BS13, $\langle S^2 \rangle$ has values of ∼9.3 in any of the S-OX models (B3LYP single-point), which is close to the "ideal" value of 9.75 for an effective doublet BS state with nine magnetic pairs (ten unpaired α and nine unpaired β electrons).[31,59] For the BS24 and BS34 models, on the other hand, $\langle S^2 \rangle \approx 8.4$, almost one unit smaller and close to the "ideal" BS value of 8.75 for nine unpaired α and eight unpaired β electrons. In direct product notation, specifying the projections onto the *z*-axis of the four site spins, where projections are maximal with respect to the site-spin quantum numbers, we thus have $|-4/2, -5/2, +5/2, +5/2\rangle$ for BS12, $|-4/2, -5/2, +5/2, +3/2\rangle$ for BS34, $|-4/2, +5/2, -5/2, +5/2\rangle$ for BS13, and $|-4/2, +5/2, -5/2, +3/2\rangle$ for BS24.

In addition to these orbital analyses, significantly shorter metal−ligand bond lengths of Fe4 in states BS34 and BS24 compared to those of experimental structure data, provide evidence of a local spin $S_4 = 3/2$ in those states. The close orbital configuration relationship between BS12 and BS34, and between BS13 and BS24 (each pair only differing by a spin-flip

DOI: 10.1021/acs.jctc.5b00854
J. Chem. Theory Comput. 2016, 12, 174−187

on Fe4), further leads to Mulliken spin populations and calculated Mössbauer quadrupole splittings for sites Fe1, Fe2, and Fe3, which are generally almost identical between orbital configuration partners, whereas these properties are markedly different between these configurations for Fe4 (see section 4.3).

The described local spin pairing on Fe4 is energetically competitive. BS24 (S_4 = 3/2) even represents the lowest state for S-OX_D^{5+} at the PBE/EPRB level, which is lower by 0.7 kcal/mol than its orbital configuration partner BS13 (S_4 = 5/2). We have to keep in mind, however, that "pure" GGA functionals like PBE tend to overstabilize lower spin states. At the B3LYP level, relative energies of BS24 models with S_4 = 3/2 are ∼6 kcal/mol higher. Results with the two functionals are expected to bracket the true preferences. To more directly probe the intrinsic preference of Fe4 for either a high-spin S_4 = 5/2 or an intermediate-spin S_4 = 3/2 or even low-spin S_4 = 1/2 state, we diamagnetically substituted $Fe1^{2+}$, $Fe2^{3+}$, and $Fe3^{3+}$ by closed-shell Zn^{2+}, Ga^{3+}, and Ga^{3+} ions, respectively, in the previously optimized BS12, BS13, and BS34 structures. Table 2 gives the computed spin-state energetics.

Table 2. Spin-State Energies (kcal/mol, PBE/B3LYP) Relative to S = 5/2 for Diamagnetically Substituted S-OX_P^{5+} Models Optimized in BS States BS12, BS13, and BS34[a]

	S = 1/2	S = 3/2	S = 5/2
BS12	+3.57/+14.01	−3.50/−1.77	0.0/0.0
BS13	+6.45/+17.43	−0.72/+1.31	0.0/0.0
BS34	−2.73/+3.76	−6.85/−7.31	0.0/0.0

[a] $Fe1^{2+}$ → Zn^{2+}, $Fe2^{3+}$ → Ga^{3+}, $Fe3^{3+}$ → Ga^{3+}, see text. Without reoptimization of the BS structures after diamagnetic substitution.

Even for substitution in the BS12 structure, both functionals provide a slight preference for a local intermediate S = 3/2 spin state. Substitution at the BS34 structure gives a clear preference of ∼7 kcal/mol for S = 3/2. That is, the BS34 structure with its shorter Fe4−N bond length is structurally adapted to S_4 = 3/2 (even S = 1/2 is below S = 5/2 at PBE level). The strong and unsymmetrical ligand field of Fe4, including hard amide (and carboxylate) ligands, provides an explanation for the close energies of local spin states at this site. Of course, the local spin is coupled to those of the other sites, and more favorable exchange interactions may outweigh local spin-state preferences in some of the BS states. Although this is difficult to disentangle in detail, we nevertheless conclude that Fe4 is relatively close to a local spin-state crossover in all of the energetically competitive BS states. Optimization of S-OX_P^{5+} with S_4 = 1/2 (without diamagnetic substitution) gives poor agreement with crystallographic data, affording a genuinely square-pyramidal five-coordinate Fe4 with a bond to Cys19 (Fe4−S(Cys19) distance of 2.29 Å) and the terminal cysteinate (Cys20) at the apex. Similarly, metal−ligand bond lengths involving Fe4 are too small in models BS24 and BS34 compared to X-ray references or the optimized BS12 or BS13 models. Another important clue comes from HYSCORE[19] and ENDOR[18] data for the ^{14}N HFC of the Cys20 amide binding to Fe4 in the S-OX state. In any conceivable coupling scheme, spin density of low-spin or intermediate-spin Fe4 would be too small to explain the experimentally found strong coupling of the ^{14}N nuclear spin to the S = 1/2 electronic spin in S-OX.

Pandelia et al.[20] reported an Fe1−Fe2 MV pair for their favored Ox2_24 model (spin-alignment corresponding to the present BS34), but otherwise, an interpretation of the electronic structure of BS34 and a rationalization of the signs of the spin-projection coefficients used in the calculation of ^{57}Fe HFCs were not provided.

4.3. Mössbauer Parameters of the Super-Oxidized State. *a. ^{57}Fe Quadrupole Splittings and Isomer Shifts.* In view of the disagreement[7,9,20−22] between previous interpretations of the Mössbauer parameters of the S-OX state (see section 2), we now computationally reinvestigate the quadrupole splittings and isomer shifts.

Considering energetics, ^{14}N HFCs, and structural data, the above discussion provided arguments against BS14, BS23, BS24, and BS34. Here, we still list calculated Mössbauer parameters for BS34 because this spin-coupling had been preferred in previous computational work (model Ox2_24[20]). However, we need to essentially concentrate on six possibilities for the most likely S-OX species studied by Mössbauer spectroscopy: S-$OX_{D\text{-}H}^{5+}$, S-OX_D^{5+}, and S-OX_P^{5+}, each in spin-couplings BS12 or BS13. The computed Mössbauer results at PBE and B3LYP levels are given in Tables 3 and 4,

Table 3. Computed Mössbauer Parameters for the S-OX_P^{5+} Model at PBE/B3LYP Levels in Different BS States As Compared to Experimental Data[a]

S-OX_P^{5+} PBE/B3LYP Mössbauer parameters					
state	site	ΔE_Q (mms^{-1})	δ (mms^{-1})	η	A_{iso}
S-OX exp.[20]	S	(+)2.45	0.46	0.5	+25.7
		(+)0.70	0.39	1.0	−47.9
		(+)0.60	0.28	0.3	+33.4
		(−)1.00	0.40	0.7	−33.6
BS12	$Fe1^{2+}$	+1.67/+2.51	0.48/0.50	0.93/0.70	+
	$Fe2^{3+}$	−0.55/−0.66	0.37/0.35	0.71/0.86	+
	$Fe3^{3+}$	−0.41/+0.47	0.32/0.29	0.89/0.95	−
	$Fe4^{3+}$	−1.63/−1.66	0.58/0.47	0.39/0.20	−
BS13	$Fe1^{2+}$	+2.51/+3.42	0.48/0.55	0.21/0.35	+
	$Fe2^{3+}$	+0.54/+0.53	0.32/0.30	0.42/0.57	−
	$Fe3^{3+}$	+0.66/+0.78	0.36/0.33	0.87/0.66	+
	$Fe4^{3+}$	−1.34/−1.26	0.59/0.50	0.85/0.85	−
BS34	$Fe1^{2+}$	+1.82/+2.70	0.50/0.51	0.69/0.50	−
	$Fe2^{3+}$	−0.54/−0.64	0.41/0.40	0.16/0.64	−
	$Fe3^{3+}$	+0.37/+0.46	0.33/0.31	0.78/0.68	+
	$Fe4^{3+}$	+2.51/+2.89	0.53/0.51	0.25/0.19	+

[a] PBE/EPRB//PBE/lacv3p** and B3LYP/EPRB//PBE/lacv3p** results. Formal iron valences are given as superscripts in the "site" column and are assigned based on the calculated {ΔE_Q} and {δ}. Only signs of A_{iso} are given. The A_{iso} are positive for "minority-spin" sites and negative for "majority-spin" sites.[60]

respectively (data for model S-$OX_{D\text{-}H}^{5+}$ is very similar to S-OX_D^{5+} and is provided in Table S17). Earlier calculated Mössbauer parameters from other groups are found in Table 1.

The consequences of the orbital configuration partnership between BS12 and BS34 (see above) are immediately apparent in the strikingly similar Mössbauer parameters predicted for Fe1, Fe2, and Fe3 in these two spin states. The EFG at the position of the Fe4 nucleus is of course very different between BS12 and BS34 due to the different spin state of Fe4 (high-spin for BS12, intermediate-spin for BS34).

Because of the opened cluster conformation in the S-OX state, only two pairs of Fe centers, Fe1−Fe2 and Fe2−Fe3, have crystallographic/calculated intermetallic distances <2.8 Å (see Table S1). Thus, only BS states BS12 and BS34 may

DOI: 10.1021/acs.jctc.5b00854
J. Chem. Theory Comput. 2016, 12, 174−187

Table 4. Computed Mössbauer Parameters for the S-OX_D^{5+} Model at PBE/B3LYP Levels in Different BS States As Compared to Experimental Data[a]

S-OX_D^{5+} PBE/B3LYP Mössbauer parameters					
state	site	ΔE_Q (mms^{-1})	δ (mms^{-1})	η	A_{iso} (MHz)
S-OX exp.[20]	S	(+)2.45	0.46	0.5	+25.7
		(+)0.70	0.39	1.0	−47.9
		(+)0.60	0.28	0.3	+33.4
		(−)1.00	0.40	0.7	−33.6
BS12	$Fe1^{2+}$	−1.56/+2.63	0.48/0.49	0.98/0.74	+
	$Fe2^{3+}$	−0.60/+0.67	0.39/0.36	0.65/0.90	+
	$Fe3^{3+}$	+0.43/+0.50	0.32/0.29	0.76/0.62	−
	$Fe4^{3+}$	−1.58/−1.78	0.33/0.28	0.70/0.83	−
BS13	$Fe1^{2+}$	+2.04/+3.10	0.44/0.50	0.42/0.46	+
	$Fe2^{3+}$	+0.49/+0.60	0.35/0.31	0.33/0.21	−
	$Fe3^{3+}$	+0.64/+0.77	0.33/0.29	0.83/0.59	+
	$Fe4^{3+}$	+1.50/+1.69	0.38/0.31	0.79/0.68	−
BS34	$Fe1^{2+}$	+1.66/+2.66	0.51/0.51	0.92/0.56	−
	$Fe2^{3+}$	−0.58/+0.60	0.41/0.37	0.81/0.88	−
	$Fe3^{3+}$	+0.38/+0.52	0.32/0.29	0.76/0.39	+
	$Fe4^{3+}$	+2.05/+2.85	0.29/0.31	0.11/0.12	+

[a]PBE/EPRB//PBE/lacv3p** and B3LYP/EPRB//PBE/lacv3p** results. Formal iron valences are given as superscripts in the "site" column and are assigned based on the calculated $\{\Delta E_Q\}$ and $\{\delta\}$. Only signs of A_{iso} are given. The A_{iso} are positive for "minority-spin" sites and negative for "majority-spin" sites.[60]

exhibit a larger degree of delocalization. A pronouncedly localized MV character of the $Fe1^{2+}$-$Fe2^{3+}$ pair in BS12 and BS34 is apparent from the calculated quadrupole splittings and isomer shifts, which are both considerably larger for Fe1 than for Fe2 at both PBE and B3LYP levels (with somewhat larger delocalization found for PBE). In models S-OX_D^{5+} and S-$OX_{D\text{-}H}^{5+}$, the computed ΔE_Q of Fe4 in state BS34 is substantially larger when using B3LYP instead of PBE.

For all three BS states, B3LYP gives ∼1 mms^{-1} larger ΔE_Q for Fe1 compared to that of the PBE results (the relative increase is larger for BS12 or BS34, where some delocalization within the Fe1−Fe2 MV pair may play a role, see above). The tendency of the B3LYP functional to overestimate quadrupole splittings in the range $\Delta E_Q > 2.0$ mms^{-1} has been described in a careful DFT calibration study of Mössbauer parameters by Lippard and co-workers[30] despite B3LYP performing well overall in that work. These differences between PBE and B3LYP prompted us to also evaluate customized B3LYP functionals with 5 and 10% of exact-exchange admixture for BS13. The resulting $\{\Delta E_Q\}$ and $\{\eta\}$ calculated with these functionals are provided in Table S24. Generally, all components of the Cartesian EFG tensors of all centers change monotonically upon increasing the amount of exact exchange from 0% (PBE) via 5% and 10% to 20% (B3LYP). In particular, the largest $\Delta E_Q > 2.5$ mms^{-1} rises with the amount of exact exchange in the functional from +2.51 mms^{-1} with PBE to +3.42 mms^{-1} with B3LYP, whereas the other (smaller) $\{\Delta E_Q\}$ remain comparably unaffected.

Focusing on the PBE results, in the following, we discuss in more detail the different BS states and models. Although we observe quite close agreement between the calculated $\{\Delta E_Q\}$ for our model BS34 S-OX_P^{5+} and the corresponding model Ox2_24 favored by Pandelia et al.[20] in terms of agreement with experimental data, the evidence provided above for a local spin $S_4 = 3/2$ leads to far too small ^{14}N hyperfine coupling.

The B3LYP results for the BS12 state S-OX_P^{5+} give Mössbauer parameters only slightly inferior to the PBE data with BS13 as well as reasonable signs of $\{A_{iso}\}$ within a "classical" spin coupling scheme. However, in view of the systematic errors of B3LYP for the largest ΔE_Q (see above),[30] which become drastically apparent in the reduced-state results reported below, we arrive at a clear preference for BS13.

Computed Mössbauer parameters for S-$OX_{D\text{-}H}^{5+}$ and S-OX_D^{5+} models are very similar, whereas differences with S-OX_P^{5+} are more pronounced. In the latter case, deprotonated Glu76 binds to Fe4, which in turn loses its bond to Cys19 (see Figure 1). Cys19 then binds terminally to Fe1 instead of assuming a μ_2-bridging mode between Fe1 and Fe4. Consequently, the Mössbauer parameters of Fe1 and Fe4 are affected much more by these structural changes than those of Fe2 or Fe3. The PBE/EPRB-level Mössbauer parameters (especially $\{\Delta E_Q\}$) for S-OX_P^{5+} in BS13 agree well with experimental data for the chosen order of assignment (cf. Table 3). We may thus assign Fe1 to site "S" and Fe4 (second-largest computed $\Delta E_Q = -1.34$ mms^{-1}) to the observed $\Delta E_Q = (-)1.00$ mms^{-1}. Uncertainties of DFT calculations as well as spectra simulations leave Fe2 and Fe3 almost indistinguishable in terms of their very similar quadrupole splittings and isomer shifts, and an earlier experimental study[9] treated these two sites as equivalent (cf. Table 1). Notwithstanding this fact, an assignment of Fe2 and Fe3 to the centers with the experimental $\Delta E_Q = (+)0.70$ and $\Delta E_Q = (+)0.60$ mms^{-1}, respectively, leads to a matching pattern of signs for $\{A_{iso}\}$. Interestingly, we did not have to invoke the measured signs of $\{A_{iso}\}$ to single out BS13 as the best approximation. This is a crucial point, because our assessment of ^{57}Fe HFCs presented in the following section suggests a reevaluation of experimental data pertaining to hyperfine couplings.

Accepting the BS13 state as the best approximation, thus supporting the conclusions of Volbeda et al. (obtained based on computed $\{\Delta E_Q\}$[7]), a clear computational distinction between the three structural models does not seem possible. The "distal" models S-$OX_{D\text{-}H}^{5+}$ and S-OX_D^{5+} overall provide slightly better isomer shifts (S-OX_P^{5+} gives a value that is somewhat too large for Fe4), but at PBE level, they underestimate the ΔE_Q of Fe1 (site S). The latter parameter depends very sensitively on the amount of exact exchange in the functional (see Table S24), and single-point calculations with 5%-HF exchange improve the ΔE_Q of Fe1 for models S-$OX_{D\text{-}H}^{5+}$ and S-OX_D^{5+}.

b. Hyperfine Couplings. The magnetic hyperfine structure from coupling of ^{57}Fe nuclear spins ($I = 1/2$) to the electronic spin of paramagnetic clusters in the applied-field Mössbauer spectra of H_2-reduced and superoxidized *Aa*-MBH was simulated with ^{57}Fe HFC tensors coaxial to each other.[20,61]

Table 5 reproduces the rhombic ^{57}Fe HFC tensors for the reduced and superoxidized proximal clusters from ref 20.

For the S-OX state, the quantity $A_{test} = -22.4$ MHz, representing the sum over all four A_{iso} values, lies in a typical range.[54] However, the dramatically anisotropic tensors for the sites with $|\Delta E_Q| = 1.00$ mms^{-1} and $|\Delta E_Q| = 0.70$ mms^{-1} (which our calculations show to be ferric) appear odd. Even before going into the spin-projected computed HFC tensors (see below), we can note here that the computed tensors (before or after scalar spin projection) do not exhibit comparably large relative anisotropies. Violation of the strong-exchange limit and a resulting modification of the anisotropies by local zero-field

DOI: 10.1021/acs.jctc.5b00854
J. Chem. Theory Comput. 2016, 12, 174−187

Table 5. Simulated ^{57}Fe HFC Tensors (in MHz, Converted from Values Given in Tesla in ref 20 by Dividing by 0.724) for the RED and S-OX State of the *Aa*-MBH Proximal Cluster from ref 20[a]

	site, ΔE_Q (mms^{-1})[b]	A_{iso}	T_{xx}	T_{yy}	T_{zz}
RED exp.	S, +2.60	+19.3	−2.8	+1.4	+1.4
	+0.84	−34.5	+13.8	−6.9	−6.9
	F, +1.52	±43.2[c]	∓1.8[d]	±0.9[d]	±0.9[d]
	+1.23	∓27.6[c]	±11.1	∓2.8	∓8.3
S-OX exp.	S, (+)2.45	+25.7	−18.6	+16.2	+2.4
	(+)0.70	−47.9	+35.1	−22.5	−12.7
	(+)0.60	+33.4	−5.8	+1.5	+4.4
	(−)1.00	−33.6	+10.1	+15.7	−25.8

[a]Effective HFC tensors are decomposed into their isotropic component A_{iso} and the anisotropic traceless part $[T_{xx}, T_{yy}, T_{zz}]$. [b]Signs of $\{\Delta E_Q\}$ for S-OX state uncertain, see caption to Table 1. [c]For the sign ambiguity, see caption to Table 1. [d]For this site, the designations $[T_{xx}, T_{yy}, T_{zz}]$ are not appropriate as the HFC tensor of Fe1 in the RED state was simulated with a principal axis system rotated with respect to the other tensors' principal axis systems; see ref 61. This is, however, a minor point given the surprisingly small anisotropy of the ferrous site S.

splitting interactions (neglected in our calculations) could be considered. However, the agreement between computed relative ^{14}N HFC anisotropies of N20 (cf. Figure 2) with ENDOR data[18,17] at the present level is excellent. For the BS13 S-OX$_P^{5+}$ model, the computed ratios of the three anisotropic ^{14}N HFC tensor components and the isotropic value are (−0.22, −0.00, +0.22) (PBE/EPRB) or (−0.19, −0.04, +0.23) (B3LYP/EPRB). This may be compared to ENDOR data of (−0.22, −0.03, +0.25). The good agreement suggests strongly that the present scalar spin projection is appropriate for S-OX (notwithstanding possible uncertainties arising from a lack of knowledge of the experimental orientation of the tensor axes). This in fact casts severe doubts on the unusually large ^{57}Fe HFC anisotropies reported for the spectra simulations.

Turning now to the explicit calculation of the ^{57}Fe HFCs for our S-OX models, we need to derive spin-projection coefficients. The localized character of the MV pair of BS13 leaves some freedom in the choice of spin-coupling schemes. From the "pure" coupling schemes (i.e., disregarding the possibility of spin canting) presented in Table 6, the requirement of having $K_4^t \approx 2$ to correctly predict the N20 ^{14}N HFCs[18,19,17] eliminates only scheme $|S_{13} = 9/2, S_{134} = 2, S_t = 1/2>$. Magnetochemical considerations based on the cluster

Table 6. Possible Spin-Coupling Schemes[a] for the S-OX State ($S_1 = 2$, $S_2 = S_3 = S_4 = 5/2$)

	K_1^t	K_2^t	K_3^t	K_4^t
$\|S_{12} = 1/2, S_{123} = 2, S_t = 1/2>$	−8/27	14/27	−14/9	7/3
$\|S_{13} = 9/2, S_{123} = 2, S_t = 1/2>$	−88/81	10/9	−110/81	7/3
$\|S_{13} = 9/2, S_{134} = 2, S_t = 1/2>$	−88/81	7/3	−110/81	10/9
$\|S_{13} = 9/2, S_{24} = 5, S_t = 1/2>$	−4/3	2	−5/3	2
$\|S_{23} = 0, S_{14} = 1/2, S_t = 1/2>$	−4/3	0	0	7/3

[a]We employ the notation $|S_A, S_B, S_t>$ as a symbolical compact notation. The "quantum numbers" S_A and S_B in general do not need to have sharp values and just denote a coupling scheme that allows for deriving the spin-projection coefficients. Signs of spin-projection coefficients $\{K_i^t\}$ correspond to the BS13 state. The $|S_{13} = 9/2, S_{134} = 2, S_t = 1/2>$ option underestimates the backbone amide ^{14}N HFC.

structure (see Figure 1, and section 2 in the Supporting Information) would favor $|S_{23} = 0, S_{14} = 1/2, S_t = 1/2>$ with $K_2^t = K_3^t = 0$. However, simulations indicated that all four Fe sites contributed to hyperfine structure in the experimental spectra.[20]

To avoid an arbitrary choice of a coupling scheme, we computed spin-projection coefficients by numerical diagonalization of the HDvV + double exchange Hamiltonian (details are given in section 4 of the Supporting Information). Computation of the isotropic exchange-coupling constants $\{J\}$ at B3LYP level (preferred here because PBE tends to overestimate isotropic exchange couplings[62]) for the BS13 S-OX$_P^{5+}$ PBE structure was performed by calculating the energies of eight different relative spin alignments. Double exchange has been accounted for, but its effect is rather small due to the clearly differentiated sites Fe1^{2+} and Fe2^{3+} of the MV pair. Regarding the (unknown) resonance delocalization parameter B for partial valence delocalization between Fe1 and Fe2 as an adjustable parameter, only J_{12} depends on B. J_{12} parametrizes the exchange interaction between localized Fe1^{2+} ($S = 2$) and Fe2^{3+} ($S = 5/2$) centers. Over the considered range for B, this model correctly predicts a doublet ground state, and the largest spin-projection coefficients, K_1^t and K_4^t, for the ground state are approximately constant over the considered range of realistic values for B, whereas K_2^t and K_3^t are in any case very small in contrast to earlier assumptions.[7,16,20] Specifically, a reasonable estimate appears to be $K_1^t = -1.16$, $K_2^t = 0.15$, $K_3^t = -0.25$, and $K_4^t = 2.28$. The spin-projection coefficients calculated explicitly in the present work are relatively close to coupling scheme $|S_{23} = 0, S_{14} = 1/2, S_t = 1/2>$.

For Fe1 (which we identify as site S), the ratios of the three traceless components and A_{iso} (Table 7) are quite close to the

Table 7. PBE/EPRB-Level Isotropic (A_{iso}) Components and Principal Values T_{ii} of the Traceless Symmetric Part of the Effective ^{57}Fe and ^{14}N Hyperfine Coupling Tensors (MHz) for S-OX$_P^{5+}$ Model in BS13 State with Spin-Projection Coefficients $K_1^t = -1.16$, $K_2^t = 0.15$, $K_3^t = -0.25$, and $K_4^t = 2.28$

	site	A_{iso}[a]	A_{iso}[b]	T_{xx}[c]	T_{yy}	T_{zz}
BS13 S-OX$_P^{5+}$	Fe1^{2+}	+12.5	N.A.	−8.3	+1.5	+6.8
	Fe2^{3+}	−2.3	−2.9	−0.3	−0.1	+0.4
	Fe3^{3+}	+4.3	+5.0	−0.5	+0.1	+0.4
	Fe4^{3+}	−49.7	−54.5	−4.7	−2.6	+7.2
	N_{C20}	+16.0	–	−3.5	+0.1	+3.5
^{14}N exp.	N_{C20}^{ENDOR}	+14.6		−3.2	−0.5	+3.6
	$N_{C20}^{HYSCORE}$	+13.0		−1.5	−1.5	+3.0

[a]Explicit spin-projected DFT results (PBE/EPRB) semiempirically scaled as described in Computational Details. Values can be compared directly to experimental data. [b]Semiempirical results from Fe$^{2.5+}$ and Fe^{3+} ionic site values and calculated 3d spin populations, see eqs 0.15 and 0.18 in Supporting Information. [c]In the calculations, the principal axis systems are different for the different HFC tensors.

simulations. However, a good match with experiment for this site would require $K_1^t \approx -2.5$, which is approximately twice that which appears realistic for this sites' spin-projection coefficient. We emphasize again that the DFT computed anisotropies for the other (ferric) sites are far from the spectra simulation data, but they appear clearly more reasonable in comparison with literature data for ferric centers in related systems.[63,64] Our scalar (strong-exchange) spin-projection

DOI: 10.1021/acs.jctc.5b00854
J. Chem. Theory Comput. 2016, 12, 174−187

scheme gives very good agreement with the principal components of the ^{14}N HFC tensor (ENDOR data) of the backbone amide binding to Fe4 in the S-OX state. It appears unlikely that this agreement is fortuitous because possible spin mixing by local zero-field splitting interactions would then have to alter the experimentally unknown ^{14}N HFC tensor orientation while keeping the principal components unchanged. Therefore, we suspect the present strong-exchange spin projection to hold to a good approximation. As DFT is known to provide accurate anisotropic ^{57}Fe HFC components, and the isotropic ^{57}Fe HFCs have been obtained in two different ways, we suggest that the experimental ^{57}Fe HFC tensors should be reevaluated, particularly with respect to the uniqueness of the fits.

4.4. Mössbauer Parameters of the Reduced State. *a. ^{57}Fe Quadrupole Splittings and Isomer Shifts.* Interpretation of the Mössbauer parameters of the six possible BS states of the RED_D^{3+} model (cf. Figure 1) is aided by the molecular structure, particularly by the intermetallic distances. The Fe3−Fe4 and Fe1−Fe3 distances are the only metal−metal distances significantly longer than ∼2.8 Å in the experimental reference data[6] and in the DFT-optimized[16] RED_D^{3+} models (Fe1−Fe3: ∼3.6 Å, Fe3−Fe4: ∼4.0 Å, see also Table S2 in ref 16 for metrics). As states BS12 and BS24 host the MV pair across these distant centers, localization is expected. This is confirmed by the calculations (valence-localization $Fe3^{3+}$-$Fe4^{2+}$ for BS12 and $Fe1^{2+}$-$Fe3^{3+}$ for BS24), which also give well-differentiated quadrupole splittings (and isomer shifts) for the two MV centers (Table 8).

Although BS34 would offer the possibility of delocalization across the Fe1-Fe2 MV pair, $Fe1^{2+}$-$Fe2^{3+}$ localization is also computationally found in this case. Overall, these observations suggest generally ferrous character for Fe1 and Fe4, leaving Fe2 or Fe3 as candidates for the "spectroscopic" site with the largest ferric character (ΔE_Q = +0.84 mms^{-1}, δ = 0.42 mms^{-1}, and a negative A_{iso}). BS14 exhibits some valence delocalization for the Fe2-Fe3 MV pair but with mainly $Fe2^{3+}$-$Fe3^{2+}$ character, as suggested by the computed Mössbauer parameters. Similarly, despite some valence delocalization, BS13 exhibits a partially localized $Fe2^{3+}$-$Fe4^{2+}$ MV pair and BS23 a corresponding $Fe1^{2+}$-$Fe4^{3+}$ MV pair. These preliminary considerations suggest Fe2 as the site corresponding to the observed ΔE_Q = +0.84 mms^{-1}.

To discuss the preferred BS states, we use a spin-coupling scheme (described below) where the MV pair determines the "majority spin".[60] Focusing first on the PBE results (Table 8), BS13 provides comparably good agreement with experimental data as model Red2_24 favored in ref 20 (which corresponds to spin coupling BS34) also when considering the signs of $\{A_{iso}\}$. These signs are different compared to the predictions of model Red2_24 but are not in conflict with spectral simulations per se (see caption to Table 1). More importantly, BS13 RED_D^{3+} and Red2_24 provide different predictions regarding the identity of spectroscopic sites "S" and "F". Although for Red2_24 Fe3 and Fe1 represent sites "S" and "F", respectively, the sites are swapped for our BS13 RED_D^{3+} model. Most notably, BS13 RED_D^{3+} closely resembles the available X-ray structures in contrast to Red2_24 (with deprotonated glutamate bound to Fe4), which differs dramatically in terms of covalent chemical bonding (see Introduction).

B3LYP single-point calculations (Table S12) again have to be viewed with caution (see above for the S-OX case): two $|\Delta E_Q|$ near 3.0 mms^{-1} result for all six BS states. A similar overestimation at B3LYP level is also implicit in the data given in ref 20 (values up to ∼4.0 mms^{-1}; Table S13[20]). In contrast, B3LYP gives rather similar results as PBE for the ferric Fe2 center of the MV pair (smallest calculated $|\Delta E_Q|$). This resembles the behavior observed for the S-OX state (see section 4.2). Intermediate exact-exchange admixtures again provide intermediate $\{\Delta E_Q\}$ for the ferrous sites, in particular in those BS states where the ferrous−ferrous pair sites are at a short distance (see Table S14; OLYP results are similar to the PBE values, Table S13).

The PBE data provide the smallest $\{\Delta E_Q\}$ values for the ferrous pair, probably too small, for BS23 and BS24 and to a lesser extent also for BS12 and BS14. BS13 and BS34 provide larger values, as their ferrous pair centers are more distant than in the other BS states. In the overall comparison between computed and experimental Mössbauer parameters, a general shortcoming is that the difference between the two largest $|\Delta E_Q|$ values (sites S and F) is computed to be only ∼0.3 mms^{-1} (except for BS24 with PBE, which however exhibits poor overall agreement), whereas it is 1.08 mms^{-1} experimentally. We assume that there are no large species-dependent differences in the structure of the reduced-state proximal cluster[16] (Mössbauer data were obtained for *Aa*-MBH, our RED_D^{3+} model derives from *Re*-MBH). Furthermore, given that the too small difference holds for any of the DFT approaches tested, we regard it as possible that the spectral simulations for the reduced state may have to be reconsidered. Indeed, a somewhat larger experimental ΔE_Q of

Table 8. Calculated Mössbauer Parameters for RED_D^{3+} in All Six BS States As Compared to Experimental Data[a]

state	site	ΔE_Q (mms^{-1})	δ (mms^{-1})	H	A_{iso} (MHz)
RED exp.[20]	S	+2.60	0.50	0.1	+19.30
		+0.84	0.42	0.3	−34.50
	F	+1.52	0.71	0.3	± 43.24
		+1.23	0.44	0.9	∓27.63
BS12	$Fe1^{2+}$	+1.87/+2.89	0.56/0.65	0.40/0.29	+
	$Fe2^{2+}$	+1.14/+2.48	0.41/0.54	0.89/0.88	+
	$Fe3^{3+}$	−0.38/-0.66	0.43/0.38	0.39/0.75	−
	$Fe4^{2+}$	+2.04/+3.12	0.61/0.68	0.62/0.40	−
BS13	$Fe1^{2+}$	+2.00/+3.11	0.51/0.57	0.32/0.29	+
	$Fe2^{3+}$	+0.92/+0.79	0.43/0.42	0.76/0.38	−
	$Fe3^{2+}$	+1.77/-3.01	0.53/0.66	0.59/0.90	+
	$Fe4^{2+}$	+1.27/+2.23	0.55/0.59	0.98/0.34	−
BS14	$Fe1^{2+}$	+1.50/+2.94	0.53/0.59	0.45/0.22	+
	$Fe2^{3+}$	+0.70/+1.16	0.42/0.46	0.18/0.34	−
	$Fe3^{2+}$	+1.26/+1.58	0.48/0.51	0.64/0.38	−
	$Fe4^{2+}$	−1.34/+3.02	0.60/0.68	0.90/0.25	+
BS23	$Fe1^{2+}$	+1.38/+1.63	0.51/0.52	0.66/0.98	−
	$Fe2^{2+}$	+1.07/+2.99	0.47/0.59	0.46/0.54	+
	$Fe3^{2+}$	+0.72/+2.86	0.53/0.61	0.30/0.63	+
	$Fe4^{3+}$	−0.81/-1.09	0.55/0.52	0.35/0.19	−
BS24	$Fe1^{2+}$	+1.86/+3.14	0.53/0.61	0.07/0.14	−
	$Fe2^{2+}$	+0.88/+2.67	0.44/0.54	0.60/0.98	+
	$Fe3^{3+}$	−0.57/-0.83	0.43/0.38	0.99/0.50	−
	$Fe4^{2+}$	+1.20/+2.97	0.64/0.71	0.11/0.18	+
BS34	$Fe1^{2+}$	−1.70/+2.63	0.48/0.53	0.91/0.80	−
	$Fe2^{3+}$	−0.54/-0.47	0.42/0.43	0.86/0.69	−
	$Fe3^{2+}$	+1.99/+3.14	0.54/0.65	0.85/0.67	+
	$Fe4^{2+}$	+1.87/+3.07	0.56/0.61	0.13/0.33	+

[a]PBE/B3LYP data with EPRB basis at PBE/lacv3p** structures.

DOI: 10.1021/acs.jctc.5b00854
J. Chem. Theory Comput. 2016, 12, 174−187

Table 9. PBE/EPRB-Level Isotropic (A_{iso}) Components and Principal Values T_{ii} of the Traceless Symmetric Part of the Effective ^{57}Fe Hyperfine Coupling Tensors (MHz) for RED$_D^{3+}$ in the BS13 State with $|S_{MV} = 9/2, S_{2+/2+} = 4, S_t = 1/2>$ Coupling Scheme

	site	A_{iso} [a]	A_{iso} [b]	$[T_{xx}, T_{yy}, T_{zz}]^{UBS}$ [c]	$[T_{xx}, T_{yy}, T_{zz}]^{PROJ}$
BS13 RED$_D^{3+}$	Fe1^{2+}	+12.5	N.A.	[−27.9, +6.4, +21.4]	[-9.3, +2.1, +7.1]
	Fe2$^{2.5+}$	−36.6	−43.0	[−9.6, −0.5, +10.1]	[−3.5, −0.2, +3.7]
	Fe3^{2+}	+22.9	N.A.	[−29.2, +10.0, +19.2]	[−9.7, +3.3, +6.4]
	Fe4$^{2.5+}$	−36.8	−44.2	[−13.2, +0.1, +13.1]	[−4.8, 0.0, +4.8]

[a]Explicit spin-projected DFT results (PBE/EPRB) semiempirically scaled as described in Computational Details. Values can be compared directly to experimental data. [b]Semiempirical results from Fe$^{2.5+}$ ionic site values and calculated 3d spin populations, see eq 0.15 in the SI. [c]In the calculations, the principal-axis systems are different for the different HFC tensors. Unrestricted broken symmetry (UBS) designates raw results prior to division by the number of unpaired electrons on the center and prior to multiplication with the spin-projection coefficient; spin-projected (PROJ) values can be compared directly to simulated data.

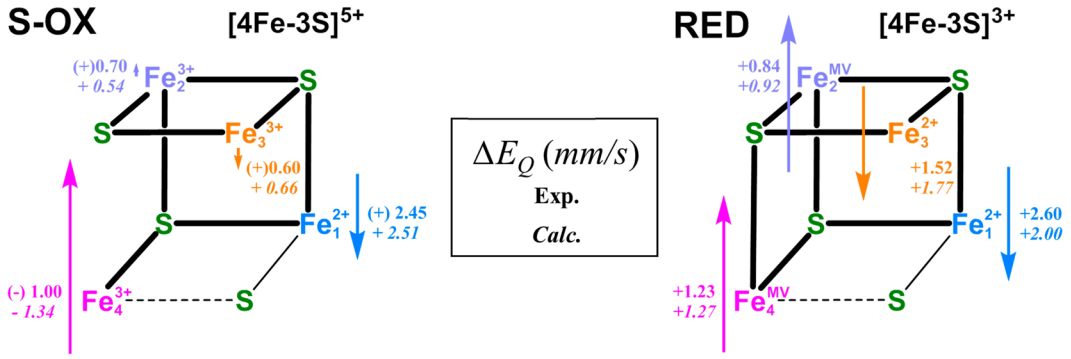

Figure 3. Summary of the main features of the electronic structure of the proximal cluster of MBH in its S-OX and RED oxidation states in terms of metal oxidation states and spin coupling. The link between "spectroscopic" metal centers and iron centers in the molecular structures is provided in terms of the quadrupole splittings, ΔE_Q. Experimental ΔE_Q values are taken from ref 20 (see Table 1 above), and calculated values refer to models BS13 S-OX$_P^{5+}$ (Table 3) and BS13 RED$_D^{3+}$ (Table 8). Spin projection coefficients K_i^t (calculated explicitly for S-OX, see Supporting Information) are represented by arrows, where ↑ and ↓ denote $K_i^t > 0$ and $K_i^t < 0$, respectively, and the length of each arrow is proportional to the magnitude of K_i^t, where $K_1^t = -1.16$ for S-OX, and so forth (see sections 4.3 and 4.4 for values of spin-projection coefficients; the scaling of arrows is the same for S-OX and RED).

site F and a somewhat smaller ΔE_Q of site S would bring the computed $\{\Delta E_Q\}$ for BS13 (PBE or B3LYP-5%) into excellent agreement with the experimental data. The computed isomer shifts at this level are somewhat too small for site F (Fe3) and somewhat too large for the site with $\Delta E_Q = +1.23$ mms^{-1} (Fe4) but should still be compatible with the combined uncertainties of the simulations and the calculations. This leaves the fit between theory and experiment for the Mössbauer parameters of the RED state less accurate than for the S-OX state but tends to favor BS13, i.e., a similar spin coupling as for the S-OX state.

b. Hyperfine Couplings. Our calculations of $\{\Delta E_Q\}$ and $\{\delta\}$ for the reduced state favor BS13 when using the PBE functional. As there is considerable delocalization within the Fe2-Fe4 MV pair in BS13 (with some predominant ferric character on Fe2), it appears justified to assume the "classical" coupling scheme $|S_{MV} = 9/2, S_{2+/2+} = 4, S_t = 1/2>$. In this scheme, Fe2 and Fe4 each have positive spin-projection coefficients ("majority spin") of 11/6, whereas Fe1 and Fe3 both have negative projection coefficients ("minority spin") of −4/3. As the intrinsic HFCs of high-spin ^{57}Fe^{3+} and ^{57}Fe^{2+} centers are always negative, multiplication with the spin-projection coefficients gives the signs $\{+, -, +, -\}$ for the effective isotropic ^{57}Fe HFCs $\{A_{iso,i}\}_{i=1\cdots4}$. These signs correspond to the upper sign option for the $\{A\}$ from the spectra simulations (cf. Table 5) when assuming a correspondence between "spectroscopic" and structural Fe centers as predicted by our BS13 RED$_D^{3+}$ model. Although the spectra could be fitted similarly well with both possible sets of signs, Pandelia et al. found satisfactory agreement with theoretical $\{\Delta E_Q\}$ and $\{\delta\}$ for model Red2_24 (criticized above) only for the $\{+, -, -, +\}$ option (sequence corresponding to the arrangement of the "RED exp." entries in Table 1). This assignment of signs $\{+, -, -, +\}$ appears to be supported by a reasonable value $A_{test} = \sum_i A_{iso,i} = -30.8$ MHz (a typical A_{test} value for Fe−S clusters falls in the range between −15 and −39 MHz[54]). However, experimental hyperfine tensors again may have to be regarded with caution. Despite the unusual coordination of Fe sites in the proximal cluster of MBH, the very small simulated hyperfine anisotropy of the ferrous sites S and—even more so—F, appear exceptional for ferrous sites in Fe−S clusters. Comparisons with Mössbauer and ENDOR data of [4Fe-4S]$^+$ clusters from ferredoxin[65] and substrate-free and substrate-bound aconitase[66,67] show ferrous sites to generally exhibit larger hyperfine anisotropy.

In Table 9, we report principal values of calculated ^{57}Fe HFC tensors to illustrate the intrinsically large (and empirically more usual) computed hyperfine anisotropies of ferrous sites S and F, now identified as Fe1 and Fe3, respectively.

Another discrepancy between calculated and simulated parameters concerns the isotropic HFCs and is illustrated by noting that our $A_{test} = -38.0$ MHz resulting from DFT calculations and spin projection differs appreciably from the estimated experimental $A_{test} = +0.4$ MHz for the $\{+, -, +, -\}$ option. We thus cautiously supply an alternative set of HFCs in Table 9 that may guide future simulations of hyperfine structure in magnetic Mössbauer or ENDOR spectra of H_2-reduced

DOI: 10.1021/acs.jctc.5b00854
J. Chem. Theory Comput. 2016, 12, 174−187

MBH with the caveat that the strong-exchange limit may not apply here.

We note in passing that the previous DFT (PBE and B3LYP) calculations of Pandelia et al.[20] for the RED and S-OX state proximal cluster overestimated the $\{A_{iso}\}$ significantly. We assume that they also used a spin-coupling scheme $|S_{MV} = 9/2, S_{2+/2+} = 4, S_t = 1/2>$ for the reduced state. This, as well as several aspects of the spin-coupling for the S-OX state, remained unclear in ref 20. However, even application of the largest conceivable magnitudes of spin-projection coefficients for pure coupling schemes cannot explain the extreme overestimation of isotropic ^{57}Fe HFCs for both S-OX and RED with several sites predicted to have $|A_{iso}| \approx 60$ MHz. Even semiempirical scaling (not detailed in ref 20) of the intrinsic isotropic Fe HFCs[68−70] could not account for such large $\{A_{iso}\}$. The HFC anisotropies should not suffer much from deficiencies in the functionals. However, those reported in ref 20 (Table S15 in that work) are also extremely large.

5. CONCLUSIONS

Our broken-symmetry DFT calculations of Mössbauer quadrupole splittings and isomer shifts in combination with the outlined spin-coupling schemes for the proximal 4Fe-3S cluster of membrane-bound hydrogenases provide good agreement with experimental data for the broken-symmetry state BS13 for both the superoxidized and reduced clusters. A concise summary of our present results pertaining to the major features of the electronic structure (metal oxidation states and spin projection coefficients) and the established correspondence between "spectroscopic metal centers" and site-specific iron centers in the molecular structure is provided in Figure 3.

Differences in the computed Mössbauer parameters for different structural models regarding the position and protonation state of the glutamate residue near Fe4 (Glu76 in *Re*-MBH) are too small to allow identification of the bonding mode of this residue based on Mössbauer spectroscopy alone. However, the present calculations resolve a previous disagreement on the assignment of Mössbauer signals to Fe sites in the superoxidized state of the cluster: they solidify the assignments of Volbeda et al.[7] rather than those of Pandelia et al.[20] Our results for the reduced state of the cluster disagree with the latter work regarding both preferred choice of broken-symmetry state and assignment of signals to the iron sites. We note that our DFT-optimized reduced-state cluster model (RED_D^{3+}) is structurally much closer to the experimental data (for *Re*-MBH) than the one used previously. The good agreement of its computed Mössbauer parameters with experiment (in BS13 state) supports its validity (including the assignment of signals to the iron sites), even though the agreement is not as close as for the superoxidized cluster. Interestingly, our calculations suggest the same type of BS state (BS13) for both superoxidized and reduced forms of the cluster, consistent with a conservation of spin coupling during the redox-induced structural transformation of the cluster. The present work supports previous notions that Fe2 remains ferric in both redox states, whereas Fe4 likely is oxidized upon (super)oxidation of the cluster (Fe1 remains ferrous). This allows us to suggest that the "special site" (S), the most distinctive feature in the Mössbauer subspectrum of the proximal cluster in all three redox states ($\Delta E_Q^{exp} = \pm 2.24$ mms^{-1} in the oxidized state), is Fe1 for all three states, in contrast to an earlier assignment. This has been possible even without using the signs of the hyperfine couplings in singling out the preferred BS state for S-OX (a comparison of computed and experimental N_{Cys20} hyperfine tensors provides additional information). We furthermore suggest that, in the superoxidized cluster, the $Fe2^{3+}$-$Fe4^{3+}$ ferric pair determines the majority spin, and the $Fe1^{2+}$-$Fe3^{3+}$ localized mixed-valence pair determines the minority spin, in contrast to the situation encountered for HiPIP's with the same set of formal metal oxidation states.[71,72]

An interesting general observation of the present study is the correspondence of pairs of broken-symmetry states regarding the distribution of formal metal oxidation states, thus forming "orbital configuration partners". Notably, the occurrence of low Fe spin populations on Fe4 in some BS states of the superoxidized cluster could be traced back to a near-degeneracy of high-spin ($S_4 = 5/2$) and intermediate-spin ($S_4 = 3/2$) local situations for this site. Although the spectroscopically detected species of the S-OX cluster clearly features an $S_4 = 5/2$ character, facile $S_4 = 5/2 \rightarrow S_4 = 3/2$ spin-crossover at Fe4 is clearly supported by the present data. It is not excluded that this may be of importance in the role of the proximal cluster in enzyme function (and possibly in oxygen tolerance).

Finally, the DFT computation of Fe hyperfine tensors followed by (scalar) spin projection has provided further insights. In the case of the superoxidized cluster, the hyperfine anisotropies obtained from the spectra simulations of Pandelia et al. appear very large. In addition, our explicit calculation of exchange couplings suggests that a ferric pair is strongly antiferromagnetically coupled, and thus the associated two sites should display only weak hyperfine coupling. Again, this point contrasts with the spectra simulations. Clearly, a reconsideration of the applied-field Mössbauer spectra is warranted. For future refined spectroscopic work addressing the proximal cluster of MBH, biochemical preparation of an enzyme lacking the [Ni-Fe] active site cluster and the [4Fe-4S] distal and [3Fe-4S] medial clusters should allow for enormous simplification of the interpretation of Mössbauer spectra. In addition, ^{57}Fe ENDOR studies appear desirable; use of the PESTRE technique[73] should allow for the determination of the absolute signs of ^{57}Fe HFCs, possibly with a higher precision and orientation selection compared with magnetic Mössbauer spectroscopy.[74]

■ ASSOCIATED CONTENT

Supporting Information

The Supporting Information is available free of charge on the ACS Publications website at DOI: 10.1021/acs.jctc.5b00854.

Test set calibrations for the calculation of isomer shifts and isotropic Fe HFCs, experimental and calculated Fe−Fe distances for the S-OX state cluster, relative energies of BS states and Mulliken spin populations of Fe sites, calculations of exchange coupling constants and projection coefficients from diagonalization of the isotropic exchange Hamiltonian + double exchange term, ^{57}Fe HFC calculation details, Mössbauer parameters for RED and S-OX B3LYP structures, and comparison of different density functionals for the calculation of quadrupole splittings for RED and S-OX models (PDF)

■ AUTHOR INFORMATION

Corresponding Author

*E-mail: martin.kaupp@tu-berlin.de.

DOI: 10.1021/acs.jctc.5b00854
J. Chem. Theory Comput. 2016, 12, 174−187

Notes

The authors declare no competing financial interest.

■ ACKNOWLEDGMENTS

The work by S.G.T., V.P., and M.K. has been carried out within the Unifying Concepts in Catalysis (UniCat) Cluster of Excellence initiative of the German Research Council (DFG) and with support by the associated Berlin International Graduate School of Natural Science and Engineering (BIG-NSE). L.N. thanks the NIH for financial support (Grant R01 GM100934) and The Scripps Research Institute for computational resources.

■ REFERENCES

(1) Lubitz, W.; Ogata, H.; Rüdiger, O.; Reijerse, E. *Chem. Rev.* **2014**, *114*, 4081−4148.
(2) Friedrich, B.; Fritsch, J.; Lenz, O. *Curr. Opin. Biotechnol.* **2011**, *22*, 358−364.
(3) Shafaat, H. S.; Rüdiger, O.; Ogata, H.; Lubitz, W. *Biochim. Biophys. Acta, Bioenerg.* **2013**, *1827*, 986−1002.
(4) Parkin, A.; Sargent, F. *Curr. Opin. Chem. Biol.* **2012**, *16*, 26−34.
(5) Shomura, Y.; Yoon, K.-S.; Nishihara, H.; Higuchi, Y. *Nature* **2011**, *479*, 253−256.
(6) Fritsch, J.; Scheerer, P.; Frielingsdorf, S.; Kroschinsky, S.; Friedrich, B.; Lenz, O.; Spahn, C. M. T. *Nature* **2011**, *479*, 249−252.
(7) Volbeda, A.; Amara, P.; Darnault, C.; Mouesca, J.-M.; Parkin, A.; Roessler, M. M.; Armstrong, F. A.; Fontecilla-Camps, J. C. *Proc. Natl. Acad. Sci. U. S. A.* **2012**, *109*, 5305−5310.
(8) The terms RED and S-OX have in ref 16 been used to denote conformations of the proximal cluster rather than redox states. In the present work, it should become clear from the context whether the cluster conformation or the redox state is meant.
(9) Pandelia, M.-E.; Nitschke, W.; Infossi, P.; Giudici-Orticoni, M.-T.; Bill, E.; Lubitz, W. *Proc. Natl. Acad. Sci. U. S. A.* **2011**, *108*, 6097−6102.
(10) Lamle, S. E.; Albracht, S. P. J.; Armstrong, F. A. *J. Am. Chem. Soc.* **2004**, *126*, 14899−14909.
(11) Vincent, K. A.; Parkin, A.; Lenz, O.; Albracht, S. P. J.; Fontecilla-Camps, J. C.; Cammack, R.; Friedrich, B.; Armstrong, F. A. *J. Am. Chem. Soc.* **2005**, *127*, 18179−18189.
(12) Volbeda, A.; Martin, L.; Cavazza, C.; Matho, M.; Faber, B. W.; Roseboom, W.; Albracht, S. P. J.; Garcin, E.; Rousset, M.; Fontecilla-Camps, J. C. *JBIC, J. Biol. Inorg. Chem.* **2005**, *10*, 239−249.
(13) Ogata, H.; Hirota, S.; Nakahara, A.; Komori, H.; Shibata, N.; Kato, T.; Kano, K.; Higuchi, Y. *Structure* **2005**, *13*, 1635−1642.
(14) Kahn, O. *Molecular Magnetism*; VCH: New York, 1993.
(15) Mouesca, J.-M.; Fontecilla-Camps, J. C.; Amara, P. *Angew. Chem., Int. Ed.* **2013**, *52*, 2002−2006.
(16) Pelmenschikov, V.; Kaupp, M. *J. Am. Chem. Soc.* **2013**, *135*, 11809−11823.
(17) Teutloff, C.; Löwenstein, J.; Fritsch, J.; Frielingsdorf, S.; Lenz, O.; Lendzian, F.; Bittl, R. In *The 45th Annual International Meeting of the ESR Spectroscopy Group of the Royal Society of Chemistry*; University of Manchster: U.K., March 25−29, 2012; p P7.
(18) Frielingsdorf, S.; Fritsch, J.; Schmidt, A.; Hammer, M.; Löwenstein, J.; Siebert, E.; Pelmenschikov, V.; Jaenicke, T.; Kalms, J.; Rippers, Y.; Lendzian, F.; Zebger, I.; Teutloff, C.; Kaupp, M.; Bittl, R.; Hildebrandt, P.; Friedrich, B.; Lenz, O.; Scheerer, P. *Nat. Chem. Biol.* **2014**, *10*, 378−385.
(19) Roessler, M. M.; Evans, R. M.; Davies, R. A.; Harmer, J.; Armstrong, F. A. *J. Am. Chem. Soc.* **2012**, *134*, 15581−15594.
(20) Pandelia, M.-E.; Bykov, D.; Izsak, R.; Infossi, P.; Giudici-Orticoni, M.-T.; Bill, E.; Neese, F.; Lubitz, W. *Proc. Natl. Acad. Sci. U. S. A.* **2013**, *110*, 483−488.
(21) Mouesca, J.-M.; Amara, P.; Fontecilla-Camps, J. C. *Proc. Natl. Acad. Sci. U. S. A.* **2013**, *110*, E2538.
(22) Pandelia, M.-E.; Bykov, D.; Izsak, R.; Infossi, P.; Giudici-Orticoni, M.-T.; Bill, E.; Neese, F.; Lubitz, W. *Proc. Natl. Acad. Sci. U. S. A.* **2013**, *110*, E2539.
(23) Papaefthymiou, V.; Girerd, J. J.; Moura, I.; Moura, J. J. G.; Münck, E. *J. Am. Chem. Soc.* **1987**, *109*, 4703−4710.
(24) Noodleman, L.; Peng, C. Y.; Case, D. A.; Mouesca, J. M. *Coord. Chem. Rev.* **1995**, *144*, 199−244.
(25) Que, L. *Physical Methods in Bioinorganic Chemistry: Spectroscopy and Magnetism*; University Science Books: Sausalito, CA, 2000.
(26) Beinert, H.; Holm, R. H.; Münck, E. *Science* **1997**, *277*, 653−659.
(27) Münck, E.; Bominaar, E. L. In *The Rudolf Mössbauer Story*; Springer: Berlin, Heidelberg, 2012; pp 243−261.
(28) Zhang, Y.; Mao, J.; Oldfield, E. *J. Am. Chem. Soc.* **2002**, *124*, 7829−7839.
(29) Neese, F. *Inorg. Chim. Acta* **2002**, *337*, 181−192.
(30) Bochevarov, A. D.; Friesner, R. A.; Lippard, S. J. *J. Chem. Theory Comput.* **2010**, *6*, 3735−3749.
(31) Sandala, G. M.; Hopmann, K. H.; Ghosh, A.; Noodleman, L. *J. Chem. Theory Comput.* **2011**, *7*, 3232−3247.
(32) Amara, P.; Mouesca, J.-M.; Volbeda, A.; Fontecilla-Camps, J. C. *Inorg. Chem.* **2011**, *50*, 1868−1878.
(33) Hay, P. J.; Wadt, W. R. *J. Chem. Phys.* **1985**, *82*, 270−283.
(34) Frisch, M. J.; Trucks, G. W.; Schlegel, H. B.; Scuseria, G. E.; Robb, M. A.; Cheeseman, J. R.; Scalmani, G.; Barone, V.; Mennucci, B.; Petersson, G. A.; Nakatsuji, H.; Caricato, M.; Li, X.; Hratchian, H. P.; Izmaylov, A. F.; Bloino, J.; Zheng, G.; Sonnenberg, J. L.; Hada, M.; Ehara, M.; Toyota, K.; Fukuda, R.; Hasegawa, J.; Ishida, M.; Nakajima, T.; Honda, Y.; Kitao, O.; Nakai, H.; Vreven, T.; Montgomery, J. A., Jr.; Peralta, J. E.; Ogliaro, F.; Bearpark, M.; Heyd, J. J.; Brothers, E.; Kudin, K. N.; Staroverov, V. N.; Kobayashi, R.; Normand, J.; Raghavachari, K.; Rendell, A.; Burant, J. C.; Iyengar, S. S.; Tomasi, J.; Cossi, M.; Rega, N.; Millam, J. M.; Klene, M.; Knox, J. E.; Cross, J. B.; Bakken, V.; Adamo, C.; Jaramillo, J.; Gomperts, R.; Stratmann, R. E.; Yazyev, O.; Austin, A. J.; Cammi, R.; Pomelli, C.; Ochterski, J. W.; Martin, R. L.; Morokuma, K.; Zakrzewski, V. G.; Voth, G. A.; Salvador, P.; Dannenberg, J. J.; Dapprich, S.; Daniels, A. D.; Farkas, Ö.; Foresman, J. B.; Ortiz, J. V; Cioslowski, J.; Fox, D. J. *Gaussian 09*, revision A. 02; Gaussian, Inc.: Wallingford, CT, 2009, *270*.
(35) Grimme, S.; Antony, J.; Ehrlich, S.; Krieg, H. *J. Chem. Phys.* **2010**, *132*, 154104.
(36) Goerigk, L.; Grimme, S. *Phys. Chem. Chem. Phys.* **2011**, *13*, 6670−6688.
(37) *Jaguar*, version 7.8; Schrödinger, LLC: New York, NY, 2011.
(38) Perdew, J. P.; Burke, K.; Ernzerhof, M. *Phys. Rev. Lett.* **1996**, *77*, 3865−3868.
(39) Perdew, J. P.; Burke, K.; Ernzerhof, M. *Phys. Rev. Lett.* **1997**, *78*, 1396.
(40) Lee, C. T.; Yang, W. T.; Parr, R. G. *Phys. Rev. B: Condens. Matter Mater. Phys.* **1988**, *37*, 785−789.
(41) Becke, A. D. *Phys. Rev. A: At., Mol., Opt. Phys.* **1988**, *38*, 3098−3100.
(42) Ahlrichs, R.; Bär, M.; Häser, M.; Horn, H.; Kölmel, C. *Chem. Phys. Lett.* **1989**, *162*, 165−169.
(43) Schäfer, A.; Horn, H.; Ahlrichs, R. *J. Chem. Phys.* **1992**, *97*, 2571−2577.
(44) Munzarová, M.; Kaupp, M. *J. Phys. Chem. A* **1999**, *103*, 9966−9983.
(45) Munzarová, M.; Kubaček, P.; Kaupp, M. *J. Am. Chem. Soc.* **2000**, *122*, 11900−11913.
(46) Kutzelnigg, W.; Fleischer, U.; Schindler, M. In *NMR Basic Principles and Progress*; Springer-Verlag: Berlin, Heidelberg, 1991; Vol. *213*, pp 165−262.
(47) Klamt, A.; Schüürmann, G. *J. Chem. Soc., Perkin Trans. 2* **1993**, *1993*, 799−805.
(48) Malkin, V.G.; Malkina, O.L.; Reviakine, R.; Arbouznikov, A.V.; Kaupp, M.; Schimmelpfennig, B.; Malkin, I.; Helgaker, T.; Ruud, K. *MAG-Respect*, version 2.1, 2007.

DOI: 10.1021/acs.jctc.5b00854
J. Chem. Theory Comput. 2016, 12, 174−187

(49) Szilagyi, R. K.; Winslow, M. A. *J. Comput. Chem.* **2006**, *27*, 1385−1397.
(50) Handy, N. C.; Cohen, A. J. *Mol. Phys.* **2001**, *99*, 403−412.
(51) Bhave, D. P.; Han, W.-G.; Pazicni, S.; Penner-Hahn, J. E.; Carroll, K. S.; Noodleman, L. *Inorg. Chem.* **2011**, *50*, 6610−6625.
(52) Hedegård, E. D.; Knecht, S.; Ryde, U.; Kongsted, J.; Saue, T. *Phys. Chem. Chem. Phys.* **2014**, *16*, 4853−4863.
(53) Long, G. J.; Grandjean, F.; Harrop, T. C.; Petroccia, H. M.; Papaefthymiou, G. C. *Inorg. Chem.* **2015**, *54*, 8415−8422.
(54) Mouesca, J.-M.; Noodleman, L.; Case, D. A.; Lamotte, B. *Inorg. Chem.* **1995**, *34*, 4347−4359.
(55) Johansson, M. P.; Sundholm, D.; Gerfen, G.; Wikström, M. *J. Am. Chem. Soc.* **2002**, *124*, 11771−11780.
(56) Sinnecker, S.; Neese, F.; Noodleman, L.; Lubitz, W. *J. Am. Chem. Soc.* **2004**, *126*, 2613−2622.
(57) Bencini, A.; Gatteschi, D. *Electron Paramagnetic Resonance of Exchange Coupled Systems*; Springer: Berlin, 1990.
(58) Schinzel, S.; Schraut, J.; Arbuznikov, A. V.; Siegbahn, P. E. M.; Kaupp, M. *Chem. - Eur. J.* **2010**, *16*, 10424−10438.
(59) Mouesca, J.-M.; Chen, J. L.; Noodleman, L.; Bashford, D.; Case, D. A. *J. Am. Chem. Soc.* **1994**, *116*, 11898−11914.
(60) The terms "majority-spin" and "minority-spin" imply positive and negative spin projection coefficients, respectively.
(61) The only exception is the site F in the reduced state cluster with one Euler angle $\beta = 40°$.
(62) Pantazis, D. A.; Orio, M.; Petrenko, T.; Zein, S.; Bill, E.; Lubitz, W.; Messinger, J.; Neese, F. *Chem. - Eur. J.* **2009**, *15*, 5108−5123.
(63) Rius, G.; Lamotte, B. *J. Am. Chem. Soc.* **1989**, *111*, 2464−2469.
(64) Dilg, A. W. E.; Mincione, G.; Achterhold, K.; Iakovleva, O.; Mentler, M.; Luchinat, C.; Bertini, I.; Parak, F. G. *JBIC, J. Biol. Inorg. Chem.* **1999**, *4*, 727−741.
(65) Middleton, P.; Dickson, D. P. E.; Johnson, C. E.; Rush, J. D. *Eur. J. Biochem.* **1978**, *88*, 135−141.
(66) Kent, T. A.; Emptage, M. H.; Merkle, H.; Kennedy, M. C.; Beinert, H.; Münck, E. *J. Biol. Chem.* **1985**, *260*, 6871−6881.
(67) Werst, M. M.; Kennedy, M. C.; Houseman, A. L.; Beinert, H.; Hoffman, B. M. *Biochemistry* **1990**, *29*, 10533−10540.
(68) Sinnecker, S.; Slep, L. D.; Bill, E.; Neese, F. *Inorg. Chem.* **2005**, *44*, 2245−2254.
(69) Fiedler, A. T.; Brunold, T. C. *Inorg. Chem.* **2005**, *44*, 9322−9334.
(70) Chakrabarti, M.; Münck, E.; Bominaar, E. L. *Inorg. Chem.* **2011**, *50*, 4322−4326.
(71) Middleton, P.; Dickson, D. P. E.; Johnson, C. E.; Rush, J. D. *Eur. J. Biochem.* **1980**, *104*, 289−296.
(72) Noodleman, L. *Inorg. Chem.* **1988**, *27*, 3677−3679.
(73) Doan, P. E. *J. Magn. Reson.* **2011**, *208*, 76−86.
(74) We are grateful to the anonymous referee that elucidated this point.

DOI: 10.1021/acs.jctc.5b00854
J. Chem. Theory Comput. 2016, 12, 174−187